Photoinduced transition from Mott insulator to metal in the undoped cuprates Nd_2CuO_4 and La_2CuO_4

H. Okamoto,[1,2,3] T. Miyagoe,[1] K. Kobayashi,[1] H. Uemura,[1] H. Nishioka,[1] H. Matsuzaki,[1] A. Sawa,[2,3] and Y. Tokura[3,4]

[1]*Department of Advanced Materials Science, University of Tokyo, Chiba 277-8561, Japan*

[2]*CREST, Japan Science and Technology Agency (JST), Chiyoda-ku, Tokyo 102-0075, Japan*

[3]*National Institute of Advanced Industrial Science and Technology (AIST), Tsukuba 305-8562, Japan*

[4]*Department of Applied Physics, University of Tokyo, Tokyo 113-8656, Japan*

(Received 29 September 2010; revised manuscript received 22 November 2010; published 9 March 2011)

Photoinduced transitions from a Mott insulator to a metal have been investigated in the undoped cuprates Nd_2CuO_4 and La_2CuO_4 by applying femtosecond pump-probe absorption spectroscopy to epitaxially grown thin-film samples. In Nd_2CuO_4, a metallic state is generated with low excitation photon density less than 0.01 photons/Cu and decays within 40 fs via the rapid photocarrier recombination. Residual photocarriers are localized by the effect of charge-spin coupling, exhibiting two midgap absorptions due to a particle and a hole. La_2CuO_4 also shows a photoinduced Mott insulator to metal transition, while it exhibits different charge dynamics from those of Nd_2CuO_4, that is, larger threshold excitation photon density for the formation of the metallic state, higher energies of the midgap absorptions, and slower recombination of polaronic carriers. These behaviors can be explained by the larger charge-phonon coupling strength in La_2CuO_4 than in Nd_2CuO_4, which is attributable to the presence of apical oxygen atoms in La_2CuO_4.

DOI: 10.1103/PhysRevB.83.125102 PACS number(s): 74.72.−h, 78.47.−p, 71.38.−k

I. INTRODUCTION

Phase controls of solids by photoirradiation are being studied extensively. This phenomenon is called a photoinduced phase transition (PIPT).[1] When we aim to realize a PIPT on a ps or sub-ps time scale, a key strategy is to use photoinduced changes of electronic structures or equivalently phase controls via purely electronic processes.[2–4] Good target materials for this purpose are Mott insulators, which are stabilized in some 3*d* transition-metal compounds and organic molecular materials. It is well known that the electronic structures of Mott insulators exhibit large variations with respect to chemical carrier doping. In fact, in various kinds of perovskite-type transition-metal oxides, Mott insulator to metal transitions are observed by chemical carrier doping. Such Mott insulator to metal transitions are called filling-control Mott transitions.[5] It is expected that similar phase transitions can also be driven by photoirradiation.[2–4] Photoinduced Mott insulator to metal transitions have been reported in one-dimensional (1D) Mott insulators such as a halogen-bridged nickel chain compound, $[Ni(chxn)_2Br]Br_2$ (chxn = cyclohexanediamine),[6] and an organic charge-transfer compound, ET-F_2TCNQ [ET = bis(ethylenedithio)tetrathiafulvalene and F_2TCNQ = difluorotetracyanoquinodimethane].[7,8] Especially in the latter compound, a Drude-like response was clearly observed by photoirradiation, which has been interpreted by the concept of the spin-charge separation characteristic of 1D strongly correlated electron systems.[9,10] A representative of the filling-control Mott transitions is observed in the layered cuprates.[11–13] The purpose of the present study is to clarify photoinduced Mott transitions (or Mott insulator to metal transitions) and photocarrier dynamics in the cuprates Nd_2CuO_4 and La_2CuO_4, which are typical parent compounds of the cuprate superconductors.

The crystal structures of Nd_2CuO_4 (Ref. 14) and La_2CuO_4 (Ref. 15) are shown in Fig. 1(a). In La_2CuO_4, each CuO plane is composed of CuO_6 octahedrons, while in Nd_2CuO_4 there are no apical oxygen atoms, which lead to simpler CuO planes. In these compounds, the Mott-Hubbard gap opens in the *d* band of copper due to the large on-site Coulomb interactions *U* at copper sites, and the occupied *p* band of oxygen is located between the upper and lower Hubbard bands of copper. Therefore, the optical gap corresponds to the charge-transfer (CT) transition from the oxygen 2*p* valence band to the copper 3*d* upper Hubbard band. Previous studies revealed that in the underdoped region of the electron-doped Nd_2CuO_4 ($Nd_{2-x}Ce_xCuO_4$) and the hole-doped La_2CuO_4 ($La_{2-x}Sr_xCuO_4$), electrons and holes cannot freely move on the antiferromagnetic (AF) spin background due to the coupling of charge and spin degrees of freedom, resulting in midgap absorptions (incoherent parts) in optical-absorption spectra.[11–13] Further carrier doping gives rise to metallic states, but the Drude weight (coherent part) is small compared to the incoherent part even under the optimum doping conditions for the highest T_c to occur.[12,13] The importance of charge-phonon coupling on doped holes has also been suggested from angle-resolved photoelectron spectra[16–20] and from optical conductivity spectra.[21] From the photoresponses of these cuprates, therefore, it is expected that we will obtain new information not only about the photoinduced Mott insulator to metal transitions but also about the nature of doped electrons and holes under the influence of charge-spin and charge-phonon couplings.[22]

Very recently, we reported the photoresponses in the thin-film samples of Nd_2CuO_4 and La_2CuO_4 in the form of a short paper,[23] in which we showed the photoinduced absorption spectra measured by a femtosecond (fs) spectroscopy with a time resolution of 200 fs, and we suggested that the photoinduced Mott transitions occur in both compounds and that charge-phonon coupling plays important roles in the dynamics during the photoinduced Mott transitions. Here, we report the comprehensive results of this study as a full paper, in which we add several important data such as the excitation-density dependence of photoinduced absorption spectra and ultrafast photoresponses investigated with a higher time resolution of

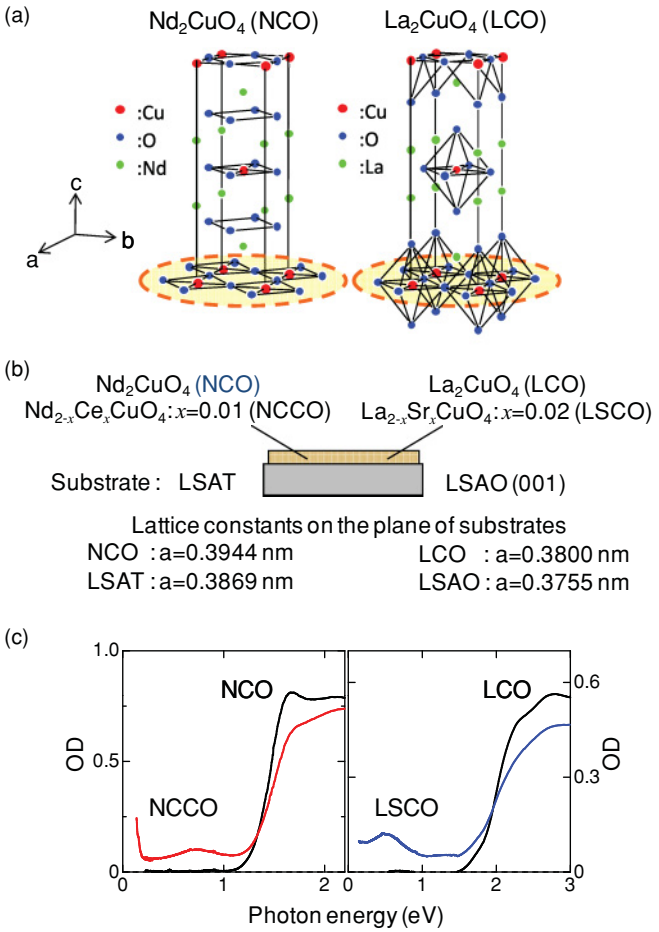

FIG. 1. (Color online) (a) Crystal structures of Nd_2CuO_4 (NCO) and La_2CuO_4 (LCO). (b) Schematic of thin-film samples and substrates. The lattice constants in the planes of the substrates are shown. (c) Optical density (OD) spectra of NCO, LCO, $Nd_{1.99}Ce_{0.01}CuO_4$ (NCCO), and $La_{1.98}Sr_{0.02}CuO_4$ (LSCO).

40 fs. The photoinduced absorption spectroscopy with the 200-fs time resolution showed that spectral shapes, time characteristics, and excitation-density dependences of photoinduced absorptions are different between La_2CuO_4 and Nd_2CuO_4. We demonstrate that these differences can be explained by the larger charge-phonon coupling in La_2CuO_4 than in Nd_2CuO_4. The photoinduced absorption measurements with the 40-fs time resolution on Nd_2CuO_4 revealed that the photoinduced metallic state decays within 40 fs via rapid photocarrier recombination and the Drude weight is almost proportional to the square of the photocarrier density. On the basis of the results, we discuss in detail charge dynamics under the influence of charge-spin and charge-phonon couplings in the cuprates. Hereafter, Nd_2CuO_4 and La_2CuO_4 are abbreviated as NCO and LCO, respectively.

II. EXPERIMENTAL DETAILS

A. Sample preparations

Thin films of NCO and LCO were grown by pulsed laser deposition on the nearly lattice-matched substrates $(LaAlO_3)_{0.3}(SrAl_{0.5}Ta_{0.5}O_3)_{0.7}$ and $LaSrAlO_4$ (001), respectively. $(LaAlO_3)_{0.3}(SrAl_{0.5}Ta_{0.5}O_3)_{0.7}$ and $LaSrAlO_4$ are abbreviated as LSAT and LSAO, respectively. Details of the growth method were reported elsewhere.[24] As reference materials, we also prepared a 1% electron-doped NCO thin film, $Nd_{1.99}Ce_{0.01}CuO_4$, and a 2% hole-doped LCO thin film, $La_{1.98}Sr_{0.02}CuO_4$, which are abbreviated as NCCO and LSCO. The thickness of the films is 120 nm in NCO and NCCO, and 100 nm in LCO and LSCO. The lattice constants of the cuprates and the substrates are shown in Fig. 1(b). Four-circle x-ray-diffraction measurements confirmed that the single-phase c-axis oriented films were epitaxially grown on LSAT and LSAO (001).

B. Femtosecond pump-probe absorption spectroscopy

For the pump-probe (PP) measurements, we used two systems with a time resolution of 200 and 40 fs, both of which were based on a Ti:Al_2O_3 regenerative amplifier (with a wavelength of 800 nm, a photon energy of 1.55 eV, a pulse width of 130 fs, and a repetition rate of 1 kHz). In the system with the time resolution of 200 fs, the output from the amplifier was divided into two beams, which were used as excitation sources for two optical parametric amplifiers (OPA's). From these two OPA's, pump (1.58 and 2.25 eV) and probe (0.1–2.2 eV) pulses were obtained. In the system with the time resolution of 40 fs, two noncollinear OPA's were excited by the outputs from the regenerative amplifier, and pump (1.72 eV) and probe (0.8–1.8 eV) pulses with the duration of ~25 fs were obtained. The delay time t_d of the probe pulse relative to the pump pulse was controlled by changing the path length of the pump pulse. The zero-time delay and the instrumental response function were determined by the cross correlation between the pump and probe pulses using a β-BaB_2O_4 crystal. The excitation photon density x_{ph} was evaluated from $x_{ph} = I_p(1-R_p)(1-1/e)/l_p$. Here, I_p, l_p, and R_p are the excitation photon density per unit area, the absorption depth, and the reflection loss of the pump light, respectively. Beams have Gaussian profiles and the diameter is 500 μm for a pump beam and 150 μm for a probe beam. All the measurements were performed at room temperature (292 K). In the measurements with the time resolution of 200 fs, photoinduced changes ΔOD of the absorption [optical density (OD)] include errors of ~5% at $t_d = 0.1$ ps due to slight variations in the temporal widths of probe pulses depending on photon energy. For $t_d > 0.2$ ps, magnitudes of errors in ΔOD are smaller than 5%. In the measurements with the time resolution of 40 fs, the temporal widths of the probe pulses were set to be nearly the same (~25 fs), so that magnitudes of errors in ΔOD are smaller than 5% in all t_d values.

III. RESULT AND DISCUSSIONS

A. Photoinduced absorption spectra and their assignments

The absorption (OD) spectra of the NCO and LCO thin films are shown in Fig. 1(c). The shoulder structures at 1.65 eV for NCO and 2.2 eV for LCO are attributable to a CT transition from the oxygen 2p valence band to the copper 3d upper-Hubbard band. The OD spectra of NCCO and LSCO are also shown in Fig. 1(c). The midgap absorptions appear

at around 0.7 eV in NCCO and at 0.5 eV in LSCO. In NCCO, the OD spectrum shows a sharp increase below 0.2 eV, attributable to the Drude-like metallic response. In LSCO, such a clear increase of the OD spectrum is not observed due to the limitation of the transparent region of the substrate (LSAO). However, the onset of the increase in OD can be seen at 0.12 eV. The absorption due to the CT transition rather decreases in both compounds, showing that the spectral weights in the gap region are transferred from the CT transitions.[12,13] In Fig. 2(a), we show the differential absorption spectra, $\Delta\mathrm{OD}_{\mathrm{NCO}}$ of NCCO and NCO, and $\Delta\mathrm{OD}_{\mathrm{LCO}}$ of LSCO and LCO, together with the OD spectra of NCO and LCO. $\Delta\mathrm{OD}_{\mathrm{NCO}}$ and $\Delta\mathrm{OD}_{\mathrm{LCO}}$ correspond to the absorption changes due to the 1%-electron doping in NCO and the 2%-hole doping in LCO, respectively.

The spectra of the photoinduced absorption changes ΔOD due to the excitation of the gap transition (1.58 eV for NCO and 2.25 eV for LCO) measured with the time resolution of 200 fs are shown in Fig. 2(b) for several delay times t_d. The excitation photon densities x_{ph} are 0.027 photons(ph)/Cu in NCO and 0.055 ph/Cu in LCO.

Here, we discuss the spectral features of ΔOD by dividing them into three regions: the infrared (IR) region for $\hbar\omega < 0.2$ eV, the near-infrared (NIR) region for $\hbar\omega > 1.0$ eV in NCO and for $\hbar\omega > 1.5$ eV in LCO, and the residual midinfrared (MIR) region. In the IR region, ΔOD at $t_d = 0.1$ ps increases monotonically with decreasing energy for both compounds, showing the Drude-like behaviors. That is,

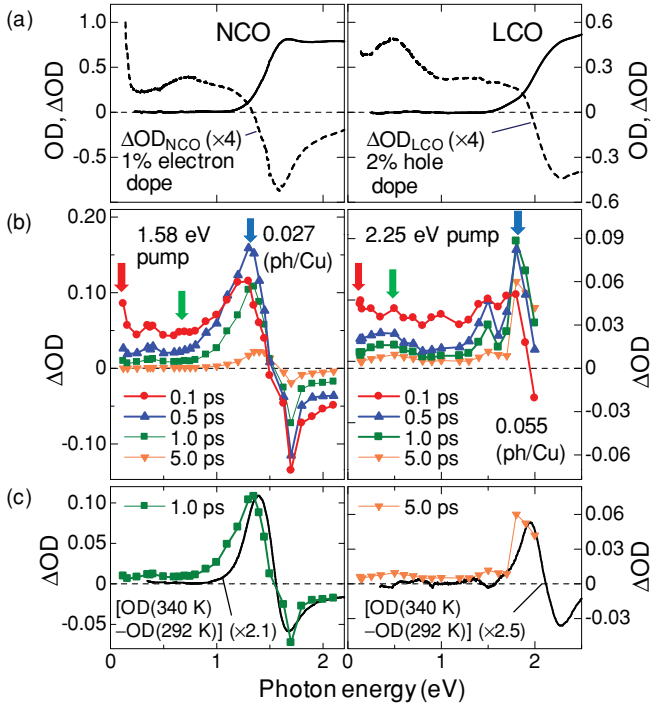

FIG. 2. (Color online) (a) OD spectra of NCO and LCO. The differential OD spectra $\Delta\mathrm{OD}_{\mathrm{NCO}}$ of NCO and NCCO and $\Delta\mathrm{OD}_{\mathrm{LCO}}$ of LCO and LSCO are also shown by broken lines. (b) Photoinduced absorption (ΔOD) spectra with pump energy of 1.58 eV ($x_{\mathrm{ph}} = 0.027$ ph/Cu) in NCO and 2.25 eV ($x_{\mathrm{ph}} = 0.055$ ph/Cu) in LCO. The time resolution is 200 fs. (c) ΔOD spectra at 1 ps of NCO and 5 ps of LCO. Solid lines show the differential OD spectra [OD(340 K)−OD (292 K)].

the metallic states are photogenerated. In the MIR region, a broad midgap absorption is observed. These photogenerated Drude-like components and midgap absorptions are similar to the absorption changes, $\Delta\mathrm{OD}_{\mathrm{NCO}}$ and $\Delta\mathrm{OD}_{\mathrm{LCO}}$, by the chemical carrier doping, which are shown in Fig. 2(a). In the NIR region, a peak structure appears at around 1.3 eV in NCO and 1.8 eV in LCO. These structures are, however, not present in NCCO and LSCO.

As for the origin of the midgap absorptions in the MIR region and the peak structures in the NIR region, the time dependence of the ΔOD spectra shown in Figs. 2(b) and 2(c) provides valuable information. The spectral shape of ΔOD changes with time in both compounds, while the decay of ΔOD is faster in NCO than in LCO: at $t_d = 1$ ps, the ΔOD signals in the IR and MIR regions almost decay in NCO but still exist in LCO [Fig. 2(b)]. In Fig. 2(c), we show the ΔOD spectra at 1 ps in NCO and at 5 ps in LCO, in which peak structures in the NIR region are distinguished as compared to the midgap absorptions. Their spectral shapes are in good agreement with the spectral changes [OD(340 K)−OD(292 K)] induced by an increase in temperature from 292 to 340 K, which were shown by solid lines in Fig. 2(c). Therefore, the ΔOD peaks in the NIR region can be attributed to the heating effects, which occur by the rapid photocarrier recombination and the thermalization of charge, spin, and lattice systems.

To further investigate the spectral changes in the MIR-to-IR region, we show in Figs. 3(a) and 3(b) expanded ΔOD spectra with a normalized scale. In both compounds, the spectral weight below 0.2 eV, that is, the Drude-like component appearing just after the photoirradiation, decreases more rapidly than the midgap absorption. These behaviors demonstrate clearly that metallic states are formed by photoirradiation and decay very fast. Then the residual carriers are localized and produce midgap absorptions, as seen in the spectra for $t_d \geqslant 2$ ps.

In both NCO and LCO, two midgap absorption peaks, **A** at 0.4 eV and **B** at ~0.7 eV in NCO and **A**′ at 0.5 eV and **B**′ at ~1.0 eV in LCO, are observed. In Figs. 3(a) and 3(b), we replotted the absorption changes due to the chemical electron doping in NCO ($\Delta\mathrm{OD}_{\mathrm{NCO}}$) and the chemical hole doping in LCO ($\Delta\mathrm{OD}_{\mathrm{LCO}}$) by the solid lines for comparison. The photoinduced absorption peak **B** in NCO corresponds well to the absorption peak in $\Delta\mathrm{OD}_{\mathrm{NCO}}$, indicating that the peak **B** is due to electron carriers. The photoinduced absorption peak **A**′ in LCO corresponds to the absorption peak in $\Delta\mathrm{OD}_{\mathrm{LCO}}$, indicating the peak **A**′ is due to hole carriers. Photoirradiation generates a pair of an electron and a hole. Consequently, it is reasonable to attribute the peak **A** in NCO and **B**′ in LCO to hole carriers and electron carriers, respectively.

By comparing the absolute values of ΔOD with $\Delta\mathrm{OD}_{\mathrm{NCO}}$ at 0.7 eV (peak **B**) in NCO and with $\Delta\mathrm{OD}_{\mathrm{LCO}}$ at 0.5 eV (peak **A**′) in LCO, we can evaluate the density of photocarriers (electrons in NCO and holes in LCO) within l_p (70 nm in NCO and 95 nm in LCO) responsible for the midgap absorptions at $t_d = 0.1$ ps to be 0.0064/Cu in NCO and 0.0071/Cu in LCO. In this evaluation, the exponential distribution of the photocarriers from the film surface to the substrate was assumed and the carrier density was averaged within l_p from the film surface. The obtained values 0.0064/Cu in NCO and 0.0071/Cu in LCO are much smaller than the excitation photon density $x_{\mathrm{ph}} = 0.027$ ph/Cu in NCO and $x_{\mathrm{ph}} = 0.055$ ph/Cu in LCO.

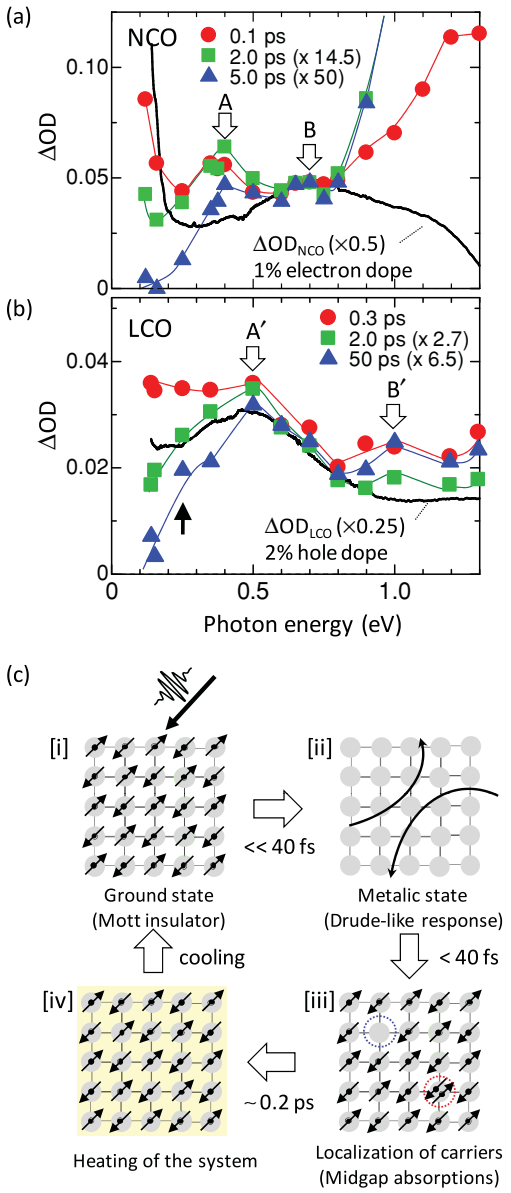

FIG. 3. (Color online) Normalized ΔOD spectra in (a) NCO (1.58 eV pump, $x_{ph} = 0.027$ ph/Cu) and (b) LCO (2.25 eV pump, $x_{ph} = 0.055$ ph/Cu). Solid lines show ΔOD_{NCO} and ΔOD_{LCO} spectra. The solid arrow indicates the phonon side band in LCO (see the text). (c) Schematic view of photoinduced phenomena in the cuprates: [i] ground state of the Mott insulator, [ii] photoinduced metallic states showing the Drude response, [iii] localized carriers showing the midgap absorption, and [iv] heating of the system after photocarrier recombinations. The characteristic times shown in the figure are deduced from the results of the 40-fs PP measurements on NCO.

This fact strongly suggests that the decay of the photoinduced metallic state is very fast and a large part of the photocarriers initially generated recombine within the time resolution of 200 fs. Note that the peak structure in the NIR region appears even at $t_d = 0.1$ ps in both compounds [see Fig. 2(b)]. This also demonstrates that photocarriers recombine within 200 fs and the heating of charge, spin, and lattice systems occurs on the subpicosecond time scale through the thermalizations.

The observed dynamics, that is, the formation and decay of the metallic state, the carrier localization process, and the heating of the system, are schematically shown in Fig. 3(c)[i]–[iv]. The characteristic times shown in Fig. 3(c) will be discussed later.

B. Nature of midgap absorptions

In this subsection, we discuss the nature of the midgap absorptions more in detail by scrutinizing the spectral shapes of ΔOD shown in Figs. 3(a) and 3(b). In the ΔOD spectra at 5 ps in NCO and 50 ps in LCO, shown by triangles in Figs. 3(a) and 3(b), respectively, the low-energy spectral weight completely disappears and the midgap absorptions due to localized carriers are observed more clearly. From a comparison of the absolute values of ΔOD with ΔOD_{NCO} or ΔOD_{LCO}, the electron and hole densities are evaluated to be 1×10^{-4}/Cu at 5 ps in NCO and 8×10^{-4}/Cu at 50 ps in LCO, respectively. The carrier densities are very small, being less than one carrier per 1000 Cu sites. Therefore, we can consider that ΔOD at 5 ps in NCO and ΔOD at 50 ps in LCO represent the spectra of isolated single-electron and single-hole states. The larger carrier density even at the larger t_d in LCO is due to the slower decay of photocarriers mentioned above. This suggests that carriers are more localized in LCO than in NCO. This point will be discussed again later.

Now, we can compare the photoinduced absorption (ΔOD) spectra to the doping-induced absorption changes expected by theoretical studies.[25–29] For the theoretical analyses of the optical-absorption spectra in doped 2D Mott insulators, the *t-J* model[25,30] has been generally used. In the cuprates, the electron-hole asymmetry exists, since the undoped compounds are CT insulators. In addition, it is known that the dynamics of charge and spin degrees of freedom and optical-absorption spectra are different between the electron-doped case and the hole-doped case.[11–13] To incorporate the differences, the *t-J* model including long-range hopping t' and t'', which is called the t-t'-t''-J model, has been adopted.[29] According to the t-t'-t''-J model, the AF spin configuration is more robust in a single-electron state than in a single-hole state.[29] This results in a higher energy of the absorption for a single-electron state than for a single-hole state. This fact can explain the energy differences between peaks **A** and **B** in NCO and between peaks **A′** and **B'** in LCO observed in the present study.

An important observation is that the energies of peaks **A′** and **B′** in LCO are relatively larger than the energies of peaks **A** and **B** in NCO, respectively. Especially, the shift of peak **B′** to the higher energy compared with peak **B** is as large as 0.3 eV. A recent theoretical study based on the *t-J* model[21] suggested that the peak structure of the midgap absorption due to a hole doping to a 2D Mott insulator originates from the charge-spin coupling and can be viewed as a magnon side band, and that the peak energy is scaled by the AF exchange interaction J. According to the results of neutron-scattering measurements, the J values of NCO and LCO were evaluated to be 155 and 133 meV, respectively.[31] Since the J value in LCO is smaller than that in NCO, the higher peak energies of **A′** and **B′** in LCO cannot be explained by the charge-spin coupling.

A possible origin for the blueshifts of the peaks **A′** and **B′** in LCO is the charge-phonon coupling. According to a

recent theoretical calculation based on the *t-J* model,[21] the introduction of the charge-phonon coupling gives rise to drastic changes in the optical conductivity spectra in a single-hole state due to polaron formations: a blueshift of the main peak due to the magnon side band, and the appearance of a shoulder structure due to the phonon side band in the lower-energy side. The former explains well the blueshift of peak **A**′ in LCO. It is natural to consider that the blueshift of peak **B**′ would also have a similar origin. The larger shift of peak **B**′ suggests that the charge-phonon coupling is more significant in an electron state than in a hole state in LCO, which will also be discussed again later. A more careful comparison of the spectral shapes of ΔOD in NCO and LCO indicates the presence of a shoulder structure at around 0.25 eV below peak **A**′ in LCO alone, as indicated by the arrow in Fig. 3(b). This may be assigned to the phonon side band.

C. Dynamical aspects of photocarriers

In this subsection, we discuss broadly the decay dynamics of photocarriers in the two cuprate compounds. The precise evaluation of the decay times of the photoinduced metallic state and photocarriers will be reported in Sec. III E, and the mechanism for the ultrafast decays will be discussed in Sec. III F.

In Fig. 4, we show time evolutions of ΔOD at 0.12 eV (0.13 eV), 0.70 eV (0.50 eV), and 1.30 eV (1.80 eV) in NCO (LCO), which reflect the dynamics of the metallic state, the midgap absorptions, and the heating effect, respectively. In both compounds, the decay of the metallic state (the ΔOD signals in the IR region) initially photogenerated is very fast. The decay time seems to be smaller than the time resolution of 200 fs. This is consistent with the fact that the magnitudes (ΔOD) of the midgap absorptions at $t_d = 0.1$ ps are much smaller than those expected from the excitation photon density x_{ph} (see Sec. III A). In contrast, the increases of the ΔOD signals at 1.3 eV in NCO and 1.80 eV in LCO by the heating

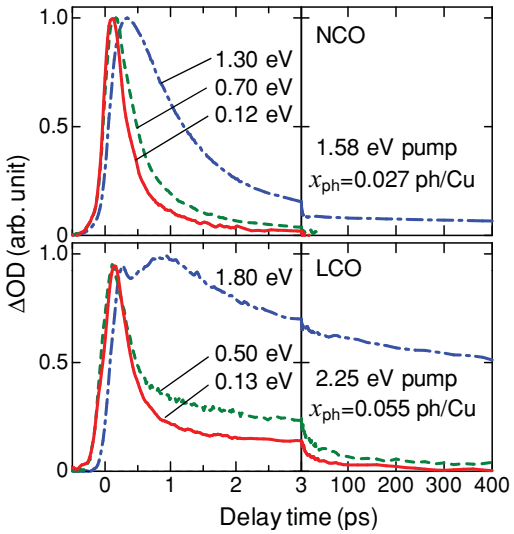

FIG. 4. (Color online) Time characteristics of ΔOD measured with the time resolution of 200 fs. The probe energies are 0.12, 0.70, and 1.30 eV in NCO, and 0.13, 0.50, and 1.80 in LCO.

are delayed in both compounds. These ΔOD signals due to the heating are long-lived up to 400 ps, as shown in Fig. 4. It was ascertained that they decay completely at least within 1 ms, which is the interval of the probe pulses.

In NCO, the decay of the midgap absorption (the ΔOD signal at 0.70 eV) is also very fast and seems to be comparable to the time resolution. However, in LCO its decay (the ΔOD signal at 0.50 eV) for $t_d > 0.3$ ps is much longer than in NCO. This can be explained by the difference in the charge-phonon coupling, which is larger in LCO than in NCO, as discussed above. When the density of photocarriers decreases and photocarriers are localized as polarons more strongly, their decay time is dominated by the encounter rate of an electron polaron and a hole polaron. The encounter rate is dominated by carriers (electrons or holes) with larger mobility. Therefore, we can consider that in LCO, both electrons and holes are stabilized as polarons and have lower mobility as compared to photocarriers in NCO. The time evolution of ΔOD at 0.50 eV in Fig. 4 shows that electron and hole polarons completely decay within 400 ps. This suggests that they are not strongly bound to the lattice but can move freely as large polarons.

D. Comparison of transient and steady-state photoinduced absorptions

The steady-state photoinduced absorption spectra measured on the powder samples of NCO (Ref. 32) and LCO (Refs. 32–34) were reported in previous studies. In the photoinduced absorption spectra measured by Kim *et al.*,[32] the two midgap absorption bands are observed in both compounds; The low-energy band (labeled as LE) was observed at 0.16 and 0.12 eV in NCO and LCO, respectively, and the high-energy band (labeled as HE) was observed at 0.62 and 0.47 eV in NCO and LCO, respectively. They suggested that the photogenerated holes in NCO and the photogenerated electrons in LCO were located outside the CuO_2 planes and that both the LE band and the HE band were due to electron polarons in NCO and hole polarons in LCO. In other words, either an electron polaron or a hole polaron generates the two midgap absorption bands, LE and HE. However, the previous photoinduced absorption spectra (the LE and HE bands) are entirely different from the absorption spectra of the chemically doped samples and our photoinduced absorption (ΔOD) spectra of the undoped samples; in the old photoinduced absorption spectra, the **A** band in NCO and the **B**′ band in LCO were not observed. In addition, the LE bands did not appear in our photoinduced absorption (ΔOD) spectra.

Another important point to be noted is that in the steady-state photoinduced absorption measurements, only the long-lived photoexcited species can be detected. On the other hand, it has been reported from several previous studies that the relaxation processes of the photoexcited states in the correlated electron systems including Mott insulators are very fast and the typical time scale of the decay times is 1 ps or less.[6,7] In the case of the cuprates, the major photoinduced changes and recovery of the electronic states are completed within 0.1 ns. The photoinduced metallic state decays within much less than 1 ps and the polarons almost decay within 100 ps, as seen in Fig. 4. In contrast, the decay times of the LE and

HE bands previously reported should be very long, being probably of the order of milliseconds. Thus, it is reasonable to consider that the steady-state photoinduced absorption studies cannot detect the intrinsic photoinduced species showing the ultrafast decay but detect only the long-lived carriers probably trapped by defects or impurities. It should be noted that the photoinduced absorption spectra reported here were measured on the high-quality single crystalline thin-film samples and the spectral information was obtained in an ultrafast time domain from femtoseconds to picoseconds. Therefore, the photoinduced absorption (ΔOD) spectra presented here detect intrinsic photocarriers and their dynamics.

E. Difference of charge-phonon coupling in NCO and LCO

In this subsection, we discuss the origin of the difference of the charge-phonon coupling in NCO and LCO. An important difference in the two compounds is that apical oxygen atoms exist in LCO but not in NCO. First, we briefly review the effects of the apical oxygen atoms on the electronic properties of the cuprates previously reported.

The most fundamental effect of the presence of apical oxygen atoms is the enhancement of the Madelung potential and the resultant increase of the CT gap energy.[35] In fact, the CT gap is larger in LCO than in NCO. However, the in-plane Cu-O distance is longer in NCO than in LCO, so that the transfer energy $t_{\rm pd}$ determined by the overlap of neighboring in-plane O $2p$ and Cu $3d$ orbitals is smaller in NCO than in LCO. This cancels the enhancement of the effective pd hybridization by the smaller CT gap in NCO. As a result, the effective pd hybridization will not be so different in the two compounds.[36] This is the reason why the values of J are almost the same in the two compounds (155 meV in NCO and 133 meV in LCO).[31]

Another important effect of the apical oxygen atoms is on the stability of doped carriers. It has been demonstrated that the apical oxygen atoms stabilize doped holes and that holes are not stabilized in NCO without apical oxygen atoms.[35] In other words, the energy of a hole is high in NCO. This is the reason why the hole-doping is very difficult in NCO. This feature will be important for the explorations and designs of materials showing high-T_c superconductivity. However, this effect is not so significant for the case of photocarrier doping. In photocarrier doping, a photoexcitation with an electronvolt scale necessarily generates a pair of an electron and a hole. The stabilization energy of a hole or an electron is never related to their generation efficiency. It will also not be related directly to the energy positions of their midgap absorption peaks. Therefore, we can discuss the energy positions of the peaks **A**($\mathbf{A}'$) and **B**($\mathbf{B}'$) by taking into account only the charge-spin coupling and the charge-phonon coupling, as discussed in Sec. III B.

From these considerations, we can consider that the effect of the apical oxygen atoms is their direct contributions to the charge-phonon coupling. A theoretical study using a cluster model suggested that the charge-phonon coupling on a doped hole due to the apical-oxygen mode is comparable to that due to the planar-oxygen mode.[20] The larger blueshift (0.3 eV) of the electron peak $\mathbf{B}'$ compared to the hole peak $\mathbf{A}'$ in LCO relative to the peaks **B** and **A** in NCO suggests that a doped electron is stabilized more strongly than a doped hole by displacements of the apical oxygen atoms. It is natural to consider that the site-diagonal-type charge-phonon coupling due to the apical oxygen atoms would play a dominant role in the stabilization of an electron carrier. This is because an electron carrier has Cu d character and should be directly affected by the displacements of apical oxygen atoms. To clarify the effects of apical oxygen atoms on the formations of hole polarons and electron polarons in more detail, a theoretical study based on the two-band model should be necessary, since the electron-hole asymmetry due to the charge-phonon coupling could not be addressed by the t-J model.

In NCO, it is natural to consider that some planar oxygen modes can also stabilize a hole similarly to the case of LCO.[20] In fact, the results of angle-resolved photoelectron spectroscopy on NCO (Ref. 37) showed characteristic spectral shapes similar to those observed in LCO, which signals the presence of a polaron effect on a hole. Thus, the charge-phonon coupling for a hole cannot be neglected in NCO, although it is weaker than in LCO, as mentioned in Sec. III B. As for the charge-phonon coupling of an electron in NCO, there has been no information expect for the fact that it is much weaker than in LCO. Theoretical studies of the optical-absorption spectra in the weakly electron-doped NCO will give definitive information about that.

F. Photodoping-density dependence of Drude components and midgap absorptions

Another important subject in the studies of the photoinduced Mott transition is a clarification of the photodoping-density dependence of the Drude components, which is one of the central issues in the Mott physics. In Fig. 5 and its insets, we show the ΔOD spectra at $t_d = 0.1$ ps for two different $x_{\rm ph}$ values; $x_{\rm ph} = 0.027$ and 0.0043 ph/Cu in NCO, and $x_{\rm ph} = 0.055$ and 0.0088 ph/Cu in LCO. In NCO, the ΔOD increases monotonically with decreasing probe photon energy for both strong (0.027 ph/Cu) and weak (0.0043 ph/Cu) excitations. Such a monotonic increase of the low-energy absorption is evidence for the photogeneration of a metallic state. Thus, in NCO, the metallic sates are formed even for the small excitation density less than 0.01 ph/Cu. In LCO, the increase of ΔOD showing a Drude-like component is observed for the strong excitation (0.055 ph/Cu), but it disappears for the weak excitation (0.0088 ph/Cu). This suggests the presence of a threshold for the photogeneration of a metallic state in LCO. This can also be attributed to the larger charge-phonon coupling in LCO. It is because the charge-phonon coupling or equivalently the polaronic effect should disturb the formation of a metallic state when the number of carriers is small.

From the discussion presented above, we can consider that NCO is a good example to evaluate the photodoping-density dependence of the Drude component characteristic of 2D Mott insulators. In NCO, the decay of the photoinduced metallic state is very fast and the time resolution of 200 fs is insufficient for the quantitative evaluations of the Drude components as seen in the time profile of ΔOD at 0.12 eV in Fig. 4. Therefore, we used the PP system with the time resolution of 40 fs. In the 40-fs system, however, IR responses could not be detected,

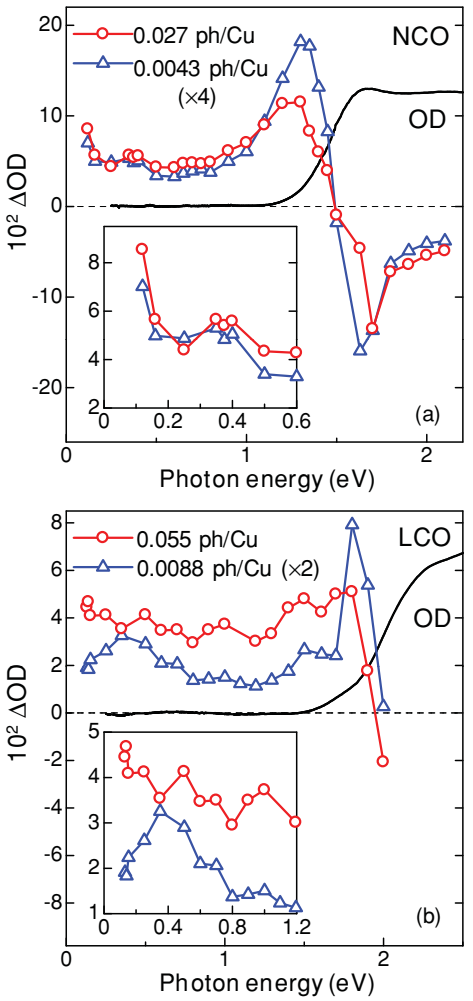

FIG. 5. (Color online) Excitation photon density dependence of ΔOD spectra just after photoirradiation (t_d = 0.1 ps) measured with the time resolution of 200 fs in (a) NCO and (b) LCO. The pump energy is 1.58 eV (x_{ph} = 0.027 ph/Cu and 0.0043 ph/Cu) in NCO and 2.25 eV (x_{ph} = 0.055 ph/Cu and 0.0088 ph/Cu) in LCO. OD spectra are also shown by solid lines in arbitrary units.

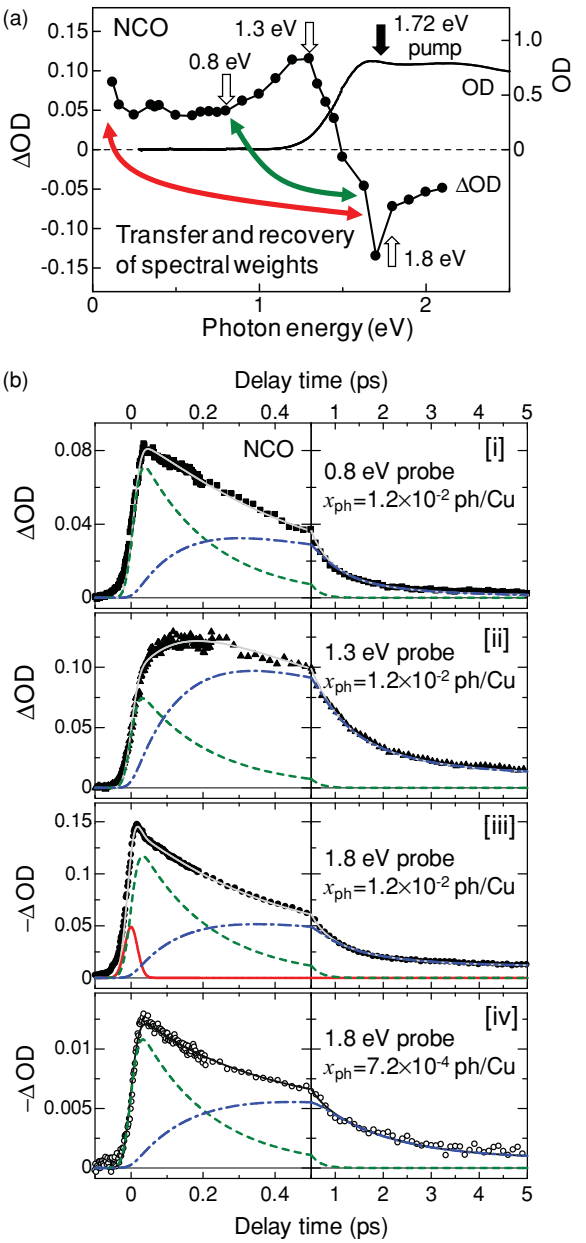

FIG. 6. (Color online) (a) OD spectrum (solid line) and ΔOD spectrum (circles) just after photoirradiation (t_d = 0.1 ps) measured with the time resolution of 200 fs and with the pump energy of 1.58 eV (x_{ph} = 0.027 ph/Cu) in NCO. [This is picked up from Fig. 2(b).] The curvilinear arrows indicate transfer and recovery of the spectral weight in the gap transition by photocarrier generation and decay, respectively. (b) Time characteristics of ΔOD measured with the time resolution of 40 fs in NCO. Pump energy is 1.72 eV, as indicated by a solid arrow in (a). Probe energies are indicated by open arrows in (a). Excitation photon densities x_{ph} are $x_{ph} = 1.2 \times 10^{-2}$ ph/Cu for [i–iii] and $x_{ph} = 7.2 \times 10^{-4}$ ph/Cu for [iv]. The gray and thin solid lines show the time characteristics obtained by the fitting procedures based upon Eq. (1). The thick-solid line, broken line, and dashed-dotted line correspond to the first, second, and third terms in Eq. (1), respectively.

since the tuning range of a noncollinear OPA is limited down to 0.75 eV. Instead, we measured the photoinduced decrease of the absorption due to the gap transition and its recovery at 1.8 eV, which is usually called a bleaching signal. This is based on the nature of the filling-control Mott transition. The filling-control Mott transition is characterized by the transfer of the spectral weight from the Mott (or CT) gap transition to the inner-gap region. The magnitude of the transferred spectral weight increases with an increase in the doping density. These features have been demonstrated by a number of studies on the chemical carrier doping to the transition-metal oxides,[5] including NCO and LCO, as shown in Figs. 1(c) and 2(a). The situation should be similar in the photodoping case. The presence of photocarriers is reflected by the bleaching signal at the region of the CT-gap transition. When photocarriers decay very fast via rapid electron-hole recombination, the spectral weight, which has been transferred from the CT-gap region to the inner-gap region, returns to the CT-gap region on the same time scale as the recombination. Such transfer and recovery of the spectral weights of the CT-gap transition is indicated by the arrows in Fig. 6(a), in which the absorption (OD) spectrum and the photoinduced absorption (ΔOD) spectrum at

t_d = 0.1 ps measured with the time resolution of 200 fs are shown. Therefore, the ultrafast response due to the photoinduced metallic state can be detected by probing the dynamics of the absorption changes (ΔOD) in the CT-gap transition region.

In the PP measurements with the time resolution of 40 fs, we selected three probe energies, 0.8, 1.3, and 1.8 eV, which reflect the absorption changes due to the midgap absorption, the heating effect, and the bleaching, respectively. In other words, only the absorption change at 1.8 eV is expected to include ultrafast components originating from photoinduced metallic states. Figure 6(b) [i]–[iii] shows the time characteristics of ΔOD at 0.8, 1.3, and 1.8 eV for the 1.72-eV pump (x_{ph} = 1.2×10^{-2} ph/Cu) measured with the time resolution of 40 fs. The sign of the vertical scale for ΔOD at 1.8 eV was reversed in Fig. 6(b) [iii] to compare its dynamics with the dynamics at the other probe energies. The initial dynamics of the ΔOD signals were shown in Figs. 7(a) and 7(b) in a normalized scale. The rise of the ΔOD signal at 1.8 eV for the 1.72-eV pump ($x_{ph} = 1.2 \times 10^{-2}$ ph/Cu) is faster than the rises at the other two energies [see Figs. 7(a) and 7(b)], indicating that an ultrafast response exists only in the bleaching signal at 1.8 eV. It is natural to consider that this ultrafast component is due to the photoinduced metallic state.

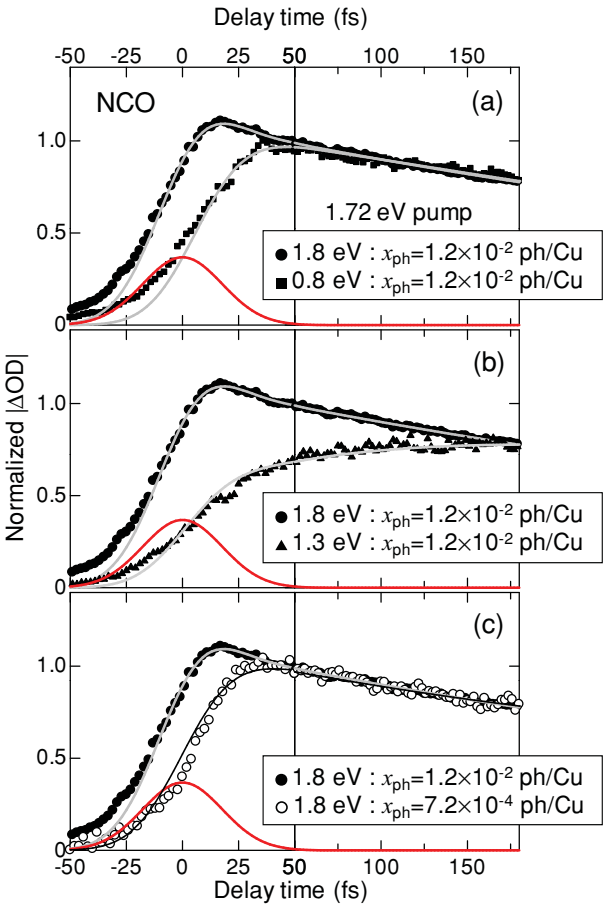

FIG. 7. (Color online) Time characteristics of |ΔOD| in the femtosecond time region normalized at t_d = 180 fs, which are the same as the data in Fig. 6(b) . In (a) and (b), ΔOD at 1.8 eV for $x_{ph} = 1.2 \times 10^{-2}$ ph/Cu is compared with |ΔOD| at 0.8 and 1.3 eV for the same excitation photon density, respectively. In (c), |ΔOD| at 1.8 eV for $x_{ph} = 1.2 \times 10^{-2}$ ph/Cu is compared with that for $x_{ph} = 7.2 \times 10^{-4}$ ph/Cu. The gray and thin solid lines show the time characteristics obtained by the fitting procedures based upon Eq. (1). The ultrafast component shown by a thick solid line corresponding to the first term in Eq. (1) is observed only in |ΔOD| at 1.8 eV for $x_{ph} = 1.2 \times 10^{-2}$ ph/Cu.

Taking these discussions into account, we derived the following formula for the analyses of the time profiles:

$$|\Delta OD| = A_1 \exp\left(-\frac{t_d^2}{\tau_0^2}\right) + A_2 \int_{-\infty}^{t_d} \exp\left(-\frac{t_d - t'}{\tau_2} - \frac{t'^2}{\tau_0^2}\right) dt' + \sum_{i=3,4} A_i \int_{-\infty}^{t_d} \left[1 - \exp\left(-\frac{t_d - t'}{\tau_2}\right)\right] \times \exp\left(-\frac{t_d - t'}{\tau_i} - \frac{t'^2}{\tau_0^2}\right) dt'. \quad (1)$$

The first term is a pulsed response attributable to the metallic state. The second term characterized by the time constant τ_2 is assigned to the midgap absorptions, and τ_2 is the decay time of photocarriers responsible for the midgap absorptions. The third term shows the delayed response due to the heating, in which the rise time is set to τ_2 and two exponential decays with time constants τ_3 and τ_4 are assumed. τ_0 (= 24 fs) is a parameter related to the pulse width. In Eq. (1), the convolution integrals with the term $\exp(-t^2/\tau_0^2)$ corresponding to the time resolution (∼40 fs) are taken into account. All of the time profiles shown in Figs. 6(b) [i]–[iii] and Figs. 7(a) and 7(b) could be well reproduced by Eq. (1), as shown by the gray lines. The used parameter values are τ_2 = 0.2 ps, τ_3 = 0.5 ps, and τ_4 = 1.5 ps. The time characteristics of three terms in Eq. (1) are shown in Fig. 6(b) [i]–[iii] by a solid line (the first term), broken lines (the second term), and the dashed-dotted lines (the third terms). The component of the first term in Eq. (1) is also shown in Figs. 7(a) and 7(b) by thick solid lines. The success of the fitting in terms of the pulsed response [the first term in Eq. (1)] and the fast decay component with the decay time of 0.2 ps [the second term in Eq. (1)] demonstrates that the metallic state decays much faster than 40 fs and the midgap absorptions decay with 0.2 ps. The characteristic times for the formation and decay of the photoinduced metallic state and the photocarrier decay in NCO were shown in Fig. 4.

In Figs. 6(b) [iv] and 7(c), we also showed the time profiles for the small excitation photon density x_{ph} of 7.2×10^{-4} ph/Cu at 1.8 eV and the fitting curves (thin solid lines) by Eq. (1). As seen in the magnified time profiles of Fig. 7(c), the ultrafast component for the stronger excitation photon density (x_{ph} = 1.2×10^{-2} ph/Cu), which was shown by the thick solid line in the figure, completely disappears. This shows that a metallic state is not photogenerated for $x_{ph} = 7.2 \times 10^{-4}$ ph/Cu. Thus, in NCO the photogeneration efficiency of metallic states seems to depend nonlinearly on the excitation photon density.

To obtain more detailed information about the excitation photon density dependence of metallic states, we performed similar analyses on time profiles at various excitation photon densities x_{ph}. Figure 8 shows the x_{ph} dependences of the maximum values of the first to third terms in Eq. (1), which are the measures of the magnitudes of the ΔOD signals

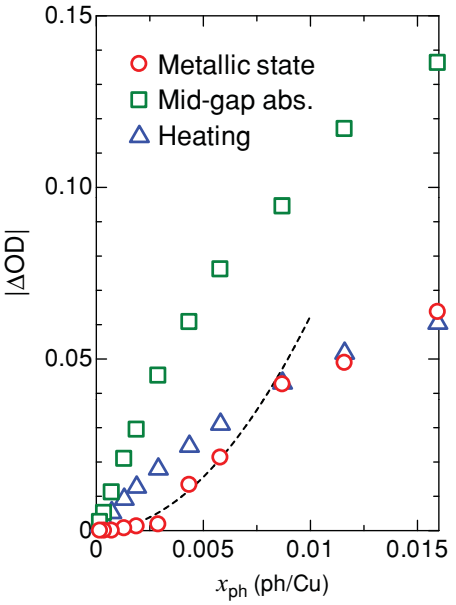

FIG. 8. (Color online) Excitation-photon-density (x_{ph}) dependence of the maximum values of |ΔOD| for the first term (circles), the second term (squares), and the third term (triangles) in Eq. (1), representing the metallic response, the midgap absorption, and the heating, respectively. The broken line shows the x_{ph}^2 dependence.

due to the metallic state, the midgap absorptions, and the heating effect. The signals due to the metallic state show nonlinear behavior for small x_{ph}. According to the analyses of the hole-doped states using the *t-J* model, the Drude weight is proportional to the square of the doped hole density x for small x.[38] The broken line in Fig. 8 shows the square dependence of absorption changes on x_{ph}, which seems to roughly reproduce the experimental x_{ph} dependence. Therefore, the square dependence of the metallic components might be characteristic of the cuprates. More strictly, in the ΔOD signals for the metallic state, a threshold behavior can be seen at around x_{ph}~0.003 ph/Cu. Below this excitation density, photocarriers might be localized more strongly due to polaronic effects, since the charge-phonon coupling would also not be negligible in NCO, as discussed in Sec. III E. In contrast, the signals due to the midgap absorptions are almost proportional to x_{ph} for small x_{ph} (<0.005 ph/Cu) and slightly saturated for larger x_{ph}. This is also consistent with the theoretical expectation based on the *t-J* model, suggesting that the total spectral weight in the inner-gap region shows a linear dependence on the doped hole density x for small x.[28]

G. Mechanism for the ultrafast decay of photocarriers

Finally, we discuss the mechanism for the ultrafast decay of the metallic state in the cuprates. In conventional semiconductors such as Si and GaAs, a strong photoexcitation generates a high density of electron and hole carriers, which gives rise to a Drude response.[39–41] The decay time of the Drude response was revealed to be several tens of picoseconds.[40,41] In contrast, the photoinduced metallic state decays within 40 fs and photocarriers responsible for the midgap absorptions decay with 200 fs in NCO, as shown in the preceding subsection. Such an ultrafast decay of the metallic state and photocarriers is the most important feature of the photoresponse in a 2D Mott insulator of NCO.

A possible explanation for the ultrafast relaxation is that photocarriers can recombine by emitting spin excitations or magnons,[42] since the charge-spin coupling is strong in the cuprates. In fact, a previous theoretical study about the photoresponse of a 2D Mott insulator showed that the spin structure rearrangement due to charge-spin coupling is an important relaxation process of the photoexcited states.[43] *J* values are large in the cuprates (155 meV in NCO and 133 meV in LCO) so that the energy of the CT-gap transition will be dissipated by emitting several quanta of magnons.

In 1D Mott insulators, photoinduced insulator-metal transitions were previously reported.[6,7] A typical example is that of an organic 1D Mott insulator, ET-F_2TCNQ,[7] in which photocarriers also decay very fast within 200 fs.[7,8] It is reasonable to consider that in the case of large U, the charge-spin coupling is much weaker in 1D Mott insulators than in 2D Mott insulators, so that another mechanism, that is, the charge-phonon coupling, might play a dominant role for the ultrafast relaxation in the 1D case. In ET-F_2TCNQ, it is known that couplings of charges with lattice phonon modes are very weak,[7] so that couplings of charges with intramolecular vibrational modes with frequencies 300–2000 cm^{-1} might play a dominant role in the ultrafast relaxation of the photoinduced metallic states and photocarriers.

In NCO, the charge-phonon coupling is weaker than in LCO, but it is still effective, as discussed in Sec. III E. In the cuprates, therefore, the charge-phonon coupling may also play important roles in the ultrafast relaxation of photocarriers. At the present stage, however, it is difficult to discriminate quantitatively the respective effects of the charge-spin coupling and the charge-phonon coupling on the relaxation processes. To clarify this point, further experimental and theoretical studies should be necessary.

IV. SUMMARY

Photoinduced Mott insulator to metal transitions and ultrafast charge dynamics due to photocarrier doping of the cuprates Nd_2CuO_4 and La_2CuO_4 were studied by applying femtosecond (fs) pump-probe absorption spectroscopy on epitaxially grown thin-film samples. In Nd_2CuO_4, a metallic state is generated with low excitation-photon density less than 0.01 photons per Cu site and decays very rapidly within 40 fs. The residual photocarriers are localized via charge-spin coupling, producing two midgap absorption peaks, which were attributed to electron carriers and hole carriers. The decay of these carriers is still fast and the decay time is evaluated to be 0.2 ps. The excitation density dependence of the photoinduced metallic states was also evaluated in Nd_2CuO_4. The decrease of the spectral weights in the gap transition due to the photogeneration of the metallic state shows a roughly quadratic dependence on the excitation photon density. In La_2CuO_4, a metallic state is also photogenerated, but the effect of charge-phonon coupling is more significant than for Nd_2CuO_4, leading to the larger threshold excitation photon density for the formation of the

metallic state, the higher energies of the midgap absorptions, and the slower recombination of polaronic carriers, compared to Nd_2CuO_4. The difference in the charge-phonon coupling of the two compounds was attributed to the fact that apical oxygen atoms exist in La_2CuO_4 and not in Nd_2CuO_4.

ACKNOWLEDGMENTS

The authors wish to thank N. Nagaosa, A. S. Mishchenko, T. Tohyama, S. Ishihara, and A. Fujimori for enlightening discussions. This work was supported in part by MEXT (16076207 and 20110005).

[1]For a review, see *Photoinduced Phase Transitions*, edited by K. Nasu (World Scientific, Singapore, 2004).
[2]H. Okamoto, S. Iwai, and H. Matsuzaki, in *Photoinduced Phase Transitions*, edited by K. Nasu (World Scientific, Singapore, 2004), pp. 239.
[3]S. Iwai and H. Okamoto, J. Phys. Soc. Jpn. **75**, 011007 (2006).
[4]H. Okamoto, in *Molecular Electronic and Related Materials—Control and Probe with Light*, edited by T. Naito (Transworld Research Network, Kerala, 2010), pp. 59–97.
[5]M. Imada, A. Fujimori, and Y. Tokura, Rev. Mod. Phys. **70**, 1039 (1998).
[6]S. Iwai, M. Ono, A. Maeda, H. Matsuzaki, H. Kishida, H. Okamoto, and Y. Tokura, Phys. Rev. Lett. **91**, 057401 (2003).
[7]H. Okamoto, H. Matsuzaki, T. Wakabayashi, Y. Takahashi, and T. Hasegawa, Phys. Rev. Lett. **98**, 037401 (2007).
[8]H. Uemura, H. Matsuzaki, Y. Takahashi, T. Hasegawa, and H. Okamoto, J. Phys. Soc. Jpn. **77**, 113714 (2008).
[9]M. Ogata and H. Shiba, Phys. Rev. B **41**, 2326 (1990).
[10]H. Eskes and A. M. Oleś, Phys. Rev. Lett. **73**, 1279 (1994).
[11]S. L. Cooper, G. A. Thomas, J. Orenstein, D. H. Rapkine, A. J. Millis, S-W. Cheong, A. S. Cooper, and Z. Fisk, Phys. Rev. B **41**, 11605 (1990).
[12]S. Uchida, T. Ido, H. Takagi, T. Arima, Y. Tokura, and S. Tajima, Phys. Rev. B **43**, 7942 (1991).
[13]Y. Onose, Y. Taguchi, K. Ishizaka, and Y. Tokura, Phys. Rev. B **69**, 024504 (2004).
[14]J. M. Longo and P. M. Raccah, J. Solid State Chem. **6**, 526 (1973).
[15]Y. Tokura, H. Takagi, and S. Uchida, Nature (London) **337**, 345 (1989).
[16]A. Lanzara, P. V. Bogdanov, X. J. Zhou, S. A. Kellar, D. L. Feng, E. D. Lu, T. Yoshida, H. Eisaki, A. Fujimori, K. Kishio, J.-I. Shimoyama, T. Noda, S. Uchida, Z. Hussain, and Z.-X. Shen, Nature (London) **412**, 510 (2001).
[17]K. M. Shen, F. Ronning, D. H. Lu, W. S. Lee, N. J. C. Ingle, W. Meevasana, F. Baumberger, A. Damascelli, N. P. Armitage, L. L. Miller, Y. Kohsaka, M. Azuma, M. Takano, H. Takagi, and Z.-X. Shen, Phys. Rev. Lett. **93**, 267002 (2004).
[18]A. S. Mishchenko and N. Nagaosa, Phys. Rev. Lett. **93**, 036402 (2004).
[19]X. J. Zhou, J. Shi, T. Yoshida, T. Cuk, W. L. Yang, V. Brouet, J. Nakamura, N. Mannella, S. Komiya, Y. Ando, F. Zhou, W. X. Ti, J. W. Xiong, Z. X. Zhao, T. Sasagawa, T. Kakeshita, H. Eisaki, S. Uchida, A. Fujimori, Z. Zhang, E. W. Plummer, R. B. Laughlin, Z. Hussain, and Z.-X. Shen, Phys. Rev. Lett. **95**, 117001 (2005).
[20]O. Rösch, O. Gunnarsson, X. J. Zhou, T. Yoshida, T. Sasagawa, A. Fujimori, Z. Hussain, Z.-X. Shen, and S. Uchida, Phys. Rev. Lett. **95**, 227002 (2005).
[21]A. S. Mishchenko, N. Nagaosa, Z.-X. Shen, G. De Filippis, V. Cataudella, T. P. Devereaux, C. Bernhard, K. W. Kim, and J. Zaanen, Phys. Rev. Lett. **100**, 166401 (2008).
[22]S. Ishihara and N. Nagaosa, Phys. Rev. B **69**, 144520 (2004).
[23]H. Okamoto, T. Miyagoe, K. Kobayashi, H. Uemura, H. Nishioka, H. Matsuzaki, A. Sawa, and Y. Tokura, Phys. Rev. B **82**, 060513(R) (2010).
[24]A. Sawa, M. Kawasaki, H. Takagi, and Y. Tokura, Phys. Rev. B **66**, 014531 (2002).
[25]T. M. Rice and F. C. Zhang, Phys. Rev. B **39**, 815 (1989).
[26]W. Stephan and P. Horsch, Phys. Rev. B **42**, 8736 (1990).
[27]J. Wagner, W. Hanke, and D. J. Scalapino, Phys. Rev. B **43**, 10517 (1991).
[28]E. Dagotto, A. Moreo, F. Ortolani, D. Poilblanc, and J. Riera, Phys. Rev. B **45**, 10741 (1992).
[29]T. Tohyama and S. Maekawa, Phys. Rev. B **64**, 212505 (2001).
[30]F. C. Zhang and T. M. Rice, Phys. Rev. B **37**, 3759 (1988).
[31]P. Bourges, H. Casalta, A. S. Ivanov, and D. Petitgrand, Phys. Rev. Lett. **79**, 4906 (1997).
[32]Y. H. Kim, S-W. Cheong, and Z. Fisk, Phys. Rev. Lett. **67**, 2227 (1991).
[33]Y. H. Kim, A. J. Heeger, L. Acedo, G. Stucky, and F. Wudl, Phys. Rev. B **36**, 7252 (1987).
[34]J. M. Ginder, M. G. Roe, Y. Song, R. P. McCall, J. R. Gaines, E. Ehrenfreund, and A. J. Epstein, Phys. Rev. B **37**, 7506 (1988).
[35]Y. Ohta, T. Tohyama, and S. Maekawa, Phys. Rev. B **43**, 2968 (1991).
[36]H. Kishida, M. Ono, A. Sawa, M. Kawasaki, Y. Tokura, and H. Okamoto, Phys. Rev. B **68**, 075101 (2003).
[37]N. P. Armitage, F. Ronning, D. H. Lu, C. Kim, A. Damascelli, K. M. Shen, D. L. Feng, H. Eisaki, Z.-X. Shen, P. K. Mang, N. Kaneko, M. Greven, Y. Onose, Y. Taguchi, and Y. Tokura, Phys. Rev. Lett. **88**, 257001 (2002).
[38]H. Tsunetsugu and M. Imada, J. Phys. Soc. Jpn. **67**, 1864 (1998).
[39]R. Huber, F. Tauser, A. Brodschelm, M. Bichler, G. Abstreiter, and A. Leitenstorfer, Nature (London) **414**, 286 (2001).
[40]M. Nagai and M. Kuwata-Gonokami, J. Phys. Soc. Jpn. **71**, 2276 (2002).
[41]R. A. Kaindl, M. A. Camahan, D. Hägele, R. Lövenich, and D. S. Chemla, Nature (London) **423**, 734 (2003).
[42]K. Matsuda, I. Hirabayashi, K. Kawamoto, T. Nabatame, T. Tokizaki, and A. Nakamura, Phys. Rev. B **50**, 4097 (1994).
[43]A. Takahashi, H. Gomi, and M. Aihara, Phys. Rev. Lett. **89**, 206402 (2002).